COLLISION-INDUCED $O^1D_2-{}^1S_0$ EMISSION NEAR 5577 Å IN ARGON*

P.S. JULIENNE, M. KRAUSS
Physical Chemistry Division, National Bureau of Standards, Washington, DC 20234, USA

and

W. STEVENS
Time and Frequency Division, National Bureau of Standards, Boulder, Colorado 80302, USA

Received 3 December 1975

The collision-induced emission near the 5577 Å oxygen $^1D_2-{}^1S_0$ transition in argon is investigated theoretically. Approximate ArO model potentials were constructed for the upper and lower states by adding the attractive long-range dispersion energy to the short-range repulsion calculated ab initio. The thermally averaged free–free, free–bound, and bound–bound contributions to the emission profile were calculated using the long-range quadrupole-induced dipole transition moment. The calculated bound–bound spectrum and the total emission coefficient agree well with experiment.

1. Introduction

Laser oscillations have recently been observed in the green emission from KrO, XeO [1], and ArO [2] excimers. This emission occurs near the wavelength of the 5577 Å atomic oxygen $^1D_2-{}^1S_0$ quadrupole line and can originate either as a continuum transition during a two-body collision of O^1S and rare gas atoms or as a transition from a weakly bound van der Waals rare gas oxide molecule formed by a three-body collision. This collision-induced oxygen emission has been suggested as a possible candidate for high energy storage laser amplifier devices [1,3]. The existence of the rare gas oxide excimer emission has long been known [4,5]. Several recent measurements have been made of the effective two-body emission coefficients of O^1S with various rare gas partners [6–9]. In spite of the current interest in the O^1S collision-induced emission in rare gases, no theory has yet been given to account for the details of this phenomenon. The present paper outlines a simple theory, specifically applied to ArO, that points out the important features that affect the emission and permits a quantitative calculation of the line shape and the total emission coefficient. First, the theoretical expressions for the rate coefficients are given. Second, the interatomic potentials and transition moment are discussed. Finally, the results of our calculation on the ArO spectrum are given and compared with experiment.

* Supported in part by Lawrence Livermore Laboratory and by the Energy Research and Development Administration.

2. Theory

2.1. Emission rate coefficients

If N_R and N_{O^*} are the number of molecules per unit volume of respective rare gas and O^1S atoms, the emission rate per unit volume per unit energy interval for photons at frequency $h\nu$ is

$$dN(h\nu)/dt = k(h\nu)N_R N_{O^*} . \quad (1)$$

The derivation of the quantum mechanical expression for $k(h\nu)$ is straightforward, following the method of Mies [10]. Let ϵ' and ϵ'' represent the respective ener-

gies of the upper state emitting level and the lower state final level. If ϵ is positive, the energy represents the kinetic energy of relative motion of the colliding pair of atoms. If ϵ is negative, its magnitude is the value of the dissociation energy of discrete bound level characterized by vibrational and rotational quantum numbers v and J. The photon energy will be expressed in terms of the shift Δ from the energy $h\nu_0$ of the unperturbed atomic line

$$\Delta = h\nu - h\nu_0 = \epsilon' - \epsilon''. \tag{2}$$

If we assume a Maxwell–Boltzmann velocity distribution and for simplicity assume the transition amplitudes for $\Delta J = \pm 1$ are the same as for $\Delta J = 0$ (this restriction is easily relaxed), the emission coefficient from the upper vibrational continuum is

$$k_f(\Delta) = \frac{64\pi^4\nu^3}{3hc^3}\frac{d''}{Q_T}\int_0^\infty d\epsilon' \sum_J (2J+1)\exp(-\epsilon'/\kappa T) \times \left[D^J_{\epsilon'\epsilon''} + \sum_{v''} D^J_{\epsilon' v''}\delta(\epsilon' - \Delta - \epsilon^J_{v''})\right]. \tag{3}$$

Here Q_T is the translational partition function $(2\pi\mu\kappa T/\hbar^2)^{3/2}$ and d'' the final state electronic degeneracy. (The initial state degeneracy is unity.) The first term in the brackets represents free–free and the second free–bound transitions. The dipole strength matrix elements are

$$D^J_{\epsilon'\epsilon''} = |\langle\epsilon' J|t(R)|\epsilon'' J\rangle|^2, \tag{4}$$

where ϵ'' can represent either a bound or a free level. The electronic transition moment $t(R)$ will be discussed later. The continuum functions for each potential are energy normalized

$$\langle\epsilon_1|\epsilon_2\rangle = \delta(\epsilon_1 - \epsilon_2), \tag{5}$$

and the bound functions are normalized to unity

$$\langle v_1|v_2\rangle = \delta_{v_1 v_2}. \tag{6}$$

At sufficiently high pressures the upper bound levels will be in thermal equilibrium with the continuum. Thus, the bound–free and bound–bound emission can be characterized by an effective two-body emission coefficient

$$k_b(\Delta) = \frac{64\pi^4\nu^3}{3hc^3}\frac{d''}{Q_T}\sum_{v'J}(2J+1)\exp(-\epsilon^J_{v'}/\kappa T) \times [D^J_{v'\epsilon''} + D^J_{v'v''}g(\Delta - \Delta^J_{v'v''})]. \tag{7}$$

Here D is defined as in (4) and $g(\Delta - \Delta^J_{v'v''})$ is the line shape factor (e.g., Doppler and/or pressure broadening) for the bound–bound emission lines. Although the contribution from the quasi-bound levels (i.e., rotational shape resonances) is formally included in $k_f(\Delta)$, it is more practical to include their effect in (7) as if they were true bound levels.

A considerable simplification can be used to obtain the total emission coefficient

$$K = \int_{-\infty}^{\infty} k(\Delta)d\Delta. \tag{8}$$

If the variation of $k(\Delta)$ from the ν^3 factor in (3) and (7) is neglected, the closure relation

$$\langle\epsilon'|[t(R)]^2|\epsilon'\rangle = \int_{-\infty}^{\infty} |\langle\epsilon'|t(R)|\epsilon''\rangle|^2 d\epsilon'' \tag{9}$$

can be applied to give the sum over all final states. The integral in (9) implies an integration over the final state continuum and a summation over the discrete levels. Neglecting the ν^3 variation is a good approximation in the present case, since the spread in Δ is very small compared to $h\nu_0$ for ArO. The results are as follows for the total free emission coefficient.

$$K_f = \frac{1}{Q_T}\frac{64\pi^4\nu_0^3}{3hc^3}\int_0^\infty d\epsilon' \exp(-\epsilon'/\kappa T)D_{\epsilon'}, \tag{10}$$

and for the total effective emission coefficient from the bound levels

$$K_b = \frac{1}{Q_T}\frac{64\pi^4\nu_0^3}{3hc^3}\sum_{v'J}\exp(-\epsilon^J_{v'}/\kappa T)(2J+1)D^J_{v'}, \tag{11}$$

where $D_{\epsilon'}$ and $D^J_{v'}$ are defined by

$$D_{\epsilon'} = \sum_J (2J+1)\langle\epsilon' J|t^2|\epsilon' J\rangle, \tag{12}$$

$$D^J_{v'} = \langle v' J|t^2|v' J\rangle. \tag{13}$$

Note that K_f and K_b depend *only* on the upper state potential and the transition moment. They are independent of the final state potential.

2.2. Potential energy curves and transition moment

A model for the interaction of a rare gas and an open-shell atom can be generalized from the model that is usually applied to the interaction of two rare gas atoms [11]. For open-shell systems charge transfer

terms dependent on the overlap must be added to the Hartree–Fock interaction energy. This is essentially equivalent to the energy of the first-order wavefunction defined by Schaefer [12]. Thus, the interaction energy is approximated by

$$E = E_{\mathrm{fo}} + E_{\mathrm{disp}}. \tag{14}$$

The purely valence contribution E_{fo} from the first-order wavefunction was calculated using the multi-configuration self-consistent-field technique of Das and Wahl [13] with accurate Hartree–Fock atomic basis sets augmented by polarization functions. The basis yields an accurate dipole polarizability of the argon atom and accounts for charge transfer to the oxygen atom. The calculated curves for ArO are shown in fig. 1. It should be noted that the quadrupole-induced dipole interaction of $O\,^1D$ with Ar is included in the calculation.

The complete potential must also include the dispersion terms, which are dominant at long range. The usual van der Waals inverse power series is used including terms through R^{-10}

$$E_{\mathrm{disp}} = -C_6/R^6 - C_8/R^8 - C_{10}/R^{10}. \tag{15}$$

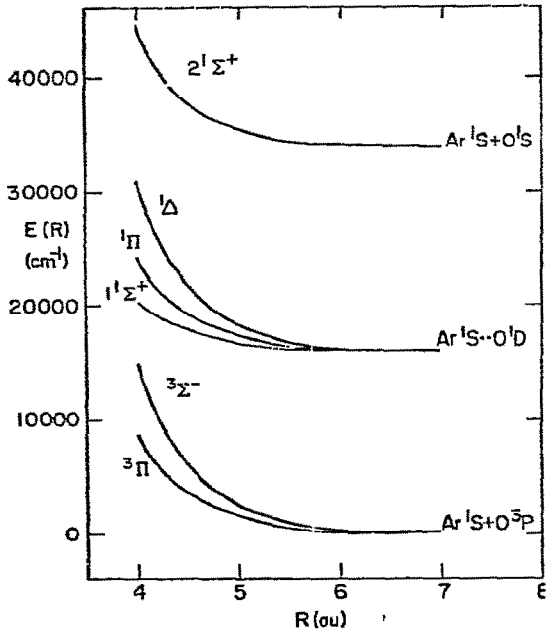

Fig. 1. Ab initio repulsive potential curves for ArO. The calculated curves have been shifted uniformly to dissociate to the correct experimental asymptotes.

This asymptotic expansion diverges at small R so that a cut-off must be applied somewhere to the left of the van der Waals minimum. Since we are concerned here only with thermal collisions which sample the potential for $R > 5$ au, no cut-off was applied. This is not believed to be a serious approximation for our purposes.

Estimates of C_6, C_8, and C_{10} were made for ArO using the Kramer–Hershbach combination formula [14], valid for both closed and open shell systems. Accurate van der Waals coefficients and static polarizabilities have been obtained by Doran [15] for the rare gases. The oxygen–oxygen C_6 coefficient is estimated from the London formula

$$C_6 = \tfrac{3}{4}\bar{\omega}_1\alpha_1^2, \tag{16}$$

where α_1 is the oxygen polarizability [16]. The value of $\bar{\omega}_1$ for oxygen is scaled by the ratio of the ionization potentials to the semi-empirical value of $\bar{\omega}_1$ for Ne obtained using Doran's value. The excited ^1D and ^1S states do not have their ionization potentials lowered by their excitation energies since spin selection rules do not permit the singlets to ionize to the $O^+\,^4S$ ion ground state. The excited state ionization potentials are thus within ≈1 eV of that for the ground state. Since the static dipole polarizability for all the oxygen states and their Λ components are very similar [16], no distinction will be made at this time in the van der Waals coefficients between the three states, ^3P, ^1D, and ^1S.

For like atom interactions the C_8 and C_{10} coefficients can be estimated from the equations [17]

$$C_8 = 3C_6\langle r^4\rangle/\langle r^2\rangle,$$

$$C_{10} = C_6[4\langle r^6\rangle/\langle r^2\rangle + \tfrac{21}{5}(\langle r^4\rangle/\langle r^2\rangle)]. \tag{17}$$

The radial matrix elements can be obtained from the tabulation of Desclaux [18]. In this way we estimate for oxygen–oxygen $C_6 = 14$, $C_8 = 183$, and $C_{10} = 3296$ in atomic units. The combination formula yields for ArO $C_6 = 30$, $C_8 = 556$, and $C_{10} = 10516$. Adding the van der Waals energy to the MC SCF results of fig. 1 yields the $1\,^1\Sigma^+$, $^1\Pi$, and $2\,^1\Sigma^+$ energy curves shown in fig. 2.

Although the theory for the interaction energy is well known, much less effort has been devoted to the theory for the induced moment. Collision-induced absorption for mixed rare gases has been analyzed theoretically by Byers-Brown and Whisnant [19]. For non-

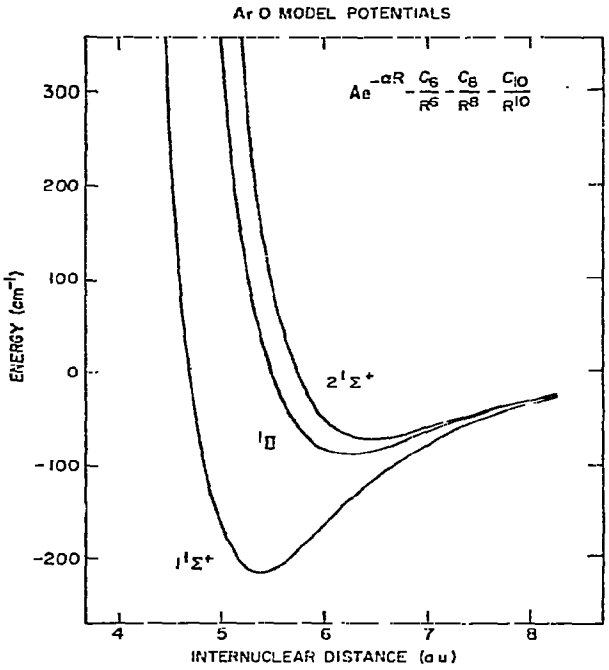

Fig. 2. Model ArO potentials shown relative to $E = 0$ at $R = \infty$.

degenerate interacting S-states the lead term in the long range expansion is the second-order induced-dipole induced-quadrupole term D_7/R^7. However, for the case of $O\,^1D$ interacting with a rare gas atom, the large permanent quadrupole moment 0.8 au of $O\,^1D$ induces a dipole moment in first order, and the lead term in the multipole series is D_4/R^4. The D_4 coefficient is simply found to be

$$D_4 = -3\alpha_D\Theta, \tag{18}$$

where α_D is the rare gas static dipole polarizability and Θ is the quadrupole moment of $O\,^1D$. Analogous expressions can be derived for the $2\,^1\Sigma^+ - 1\,^1\Sigma^+$ and $2\,^1\Sigma^+ - 1\,^1\Pi$ dipole transition moments $t(R) = T_4/R^4$, since both first-order wavefunctions are orthogonal. The results are

$$T_4(\Sigma-\Sigma) = -3\alpha_D\langle O(^1S)|\Theta_0|O(^1D)\rangle \tag{19}$$

and

$$T_4(\Sigma-\Pi) = 3^{-1/2}T_4(\Sigma-\Sigma). \tag{20}$$

The coefficients D_4 and T_4 are readily calculated for all the rare gases interacting with all group VIA elements. The dipole polarizabilities of the rare gases have been measured [20] and the quadrupole moments of oxygen-like atoms are proportional to the matrix element $\langle r^2\rangle$ for the open shell p-type electron. Table 1 gives D_4 in atomic units for the $^1D(^1\Sigma^+)$ state. If the small variation of the p-orbital between ^1D and ^1S is neglected, the $2\,^1\Sigma^+ - 1\,^1\Sigma^+$ transition moment coefficient is simply related to D_4

$$T_4 = 2^{1/2}D_4. \tag{21}$$

Table 1
$-D_4(^1D(^1\Sigma^+))^{a)}$

	He	Ne	Ar	Kr	Xe
O	3.33	6.42	26.7	40.3	65.6
S	8.49	16.3	67.9	102	167
Se	10.1	19.4	80.8	122	199
Te	13.0	25.0	103.8	157	255

a) In atomic units (ea_0).

The long-range perturbation formula can be compared directly with the ab initio results for ArO. At $R = 8$ au the perturbation expression predicts a dipole moment of 0.0065 au for the $1\,^1\Sigma^+$ state. This is in excellent agreement with the calculated dipole moment of 0.0066 au. The negative D_4 coefficient implies a polarity of Ar^+O^-, as obtained by the ab initio calculation.

An accurate calculation of the rare gas oxide excimer emission must also consider overlap effects on the transition moment. At distances shorter than some distance to the right of the van der Waals minimum in the upper state, the overlapping of the two wavefunctions will cause the true transition moment to depart from its long range perturbation form. The effect of this overlap will be to *increase* the $\Sigma-\Sigma$ transition moment and *decrease* the $\Sigma-\Pi$ moment. Since the transition moment is only required for $R > 5$ au, the quadrupole induced-dipole term is sufficient for a qualitative characterization of the rare gas oxide excimer emission.

3. Results for the ArO spectrum

Approximate model potentials were constructed for the $2\,^1\Sigma^+$, $1\,^1\Sigma^+$, and $^1\Pi$ states of ArO by adding the dispersion terms to an exponential repulsive potential

$Ae^{-\alpha R}$ found by fitting to the ab initio potential between 5 and 7 au. The ab initio potentials are all closely approximated by the exponential form for $R > 5$ au. With these potentials the integrals (4), (12) and (13) were evaluated numerically using Gordon's algorithm [21] for the bound and continuum wavefunctions. The emission line shapes $k(\Delta)$ and the total emission coefficient K were calculated using the long range transition moment. Although the contribution from the quasi-bound levels was not explicitly calculated, their estimated effect is included in the discussion below.

The respective $2\,^1\Sigma^+$, $1\,^1\Sigma^+$, and $^1\Pi$ model potentials have 4, 6, and 4 bound levels for $J = 0$ (not including the long range levels within ≈ 1 cm^{-1} of the dissociation limit). The respective $v = 0$–3 $2\,^1\Sigma^+$ vibrational levels have 22, 17, 12, and 7 bound rotational levels. The number of quasi-bound levels will be ≈40% of the number of bound levels. At the temperature of liquid nitrogen 44% of the calculated total collision-induced emission originates from the upper bound levels, but only 6% at room temperature and 2% at 600 K. The quasi-bound levels are expected to contribute less to the total emission than the bound levels, although their contribution can be a significant fraction of that of the bound levels, perhaps as much as half, depending on temperature.

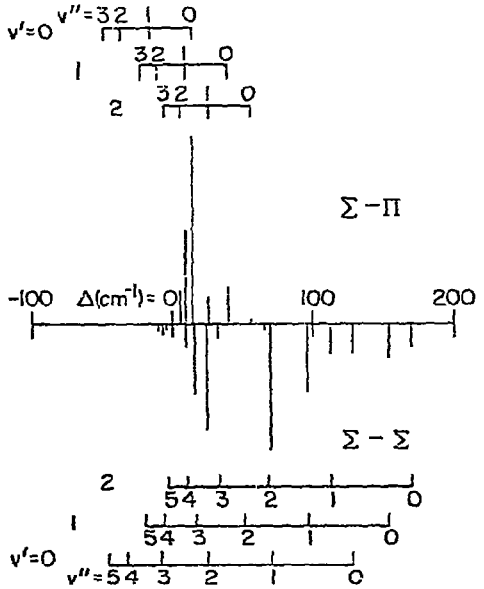

Fig. 3. Calculated ArO emission spectrum for $J = 0$. The vertical coordinate indicates relative intensities and the horizontal coordinate shows the band origins.

Banded emission spectra near 5577 Å have long been known to exist for argon, krypton, and xenon oxides [4,5]. Cooper and Lichtenstein [4] list apparent band heads for ArO and say they resolve some 130 rotational lines, although they were unable to obtain rotational assignments. Fig. 3 shows the Σ–Σ and Σ–Π band origins and relative intensities $|\langle v'|r(R)|v''\rangle|^2$ calculated with $J = 0$ for our model potentials. This figure does not include thermal differences.

Since the $2\,^1\Sigma^+$ and $^1\Pi$ potentials are so similar in shape, the dominant Σ–Π transitions are predicted to be (0,0) and (1,1) which will lie slightly to the blue of the atomic line and be shaded to the red. This agrees well with Cooper's very strong features with band heads at $\Delta = 5.6$ and 3.0 cm^{-1} [4]. These Σ–Π transitions appear very intense due to extensive line overlapping. The entire (0,0) R branch is predicted to span only ≈3 cm^{-1} before breaking off near $J \approx 28$ from strong rotational predissociation in the upper state. The respective (0,0) Q and P branches are predicted to span 9 and 16 cm^{-1} before breaking off. This is in good agreement with the span of lines to the red of 5577 Å evident in Cooper's published photograph of the spectrum [4].

Although the Σ–Σ transition moment is larger than that for Σ–Π, the Σ–Σ bands appear less intense since the transition is spread over more vibrational bands and the rotational lines are much less overlapped than for the Σ–Π transition. The calculated and experimental Σ–Σ spectra seem generally consistent. The extremely weak feature farthest to the blue in Cooper's spectrum occurs at $\Delta = 169$ cm^{-1}, as compared to our calculated (2,0) and (3,0) band origins of 170 and 179 cm^{-1} respectively. The two stronger experimental features other than the two Σ–Π transitions near the atomic line are at $\Delta = 18$ and 69 cm^{-1}. These correspond well with the two strongest predicted Σ–Σ transitions, the (0,2) and (0,1) at $\Delta = 24$ and 70 cm^{-1} respectively.

Although bound–free emission is possible, application of the closure relation shows that almost all of the emission from the upper bound levels is bound–bound. Therefore, the bound–free spectrum, which occurs to the red of the atomic line, was not calculated.

The calculated line shape $k(\Delta)$ at 300 K in units of cm^3 s^{-1} Hz^{-1} = cm^3 is shown in fig. 4. The emission near $\Delta = 0$ comes primarily from long range collisions, and the Σ–Σ and Σ–Π intensities are similar in magnitude. The long blue tail of the emission is almost entire-

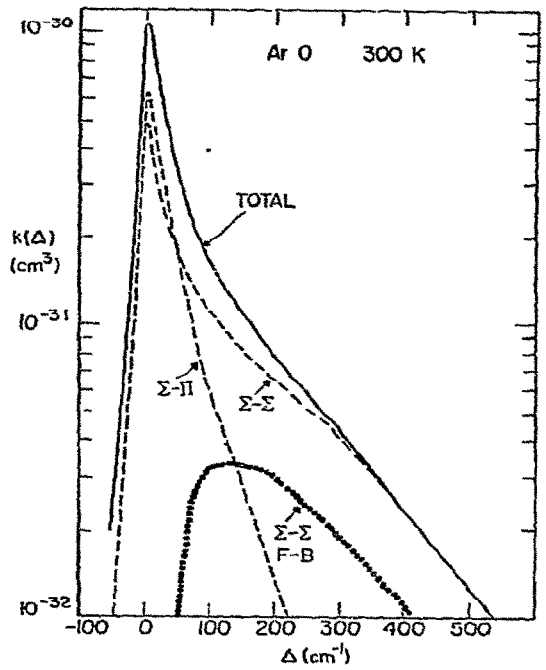

Fig. 4. Calculated 300 K ArO emission profile $k(\Delta)$ in $cm^3\ s^{-1}\ Hz^{-1}$. The individual Σ -Σ and Σ -Π contributions are shown, as well as the Σ–Σ free–bound contribution.

ly due to the Σ–Σ transition, as obviously must be the case from applying the Franck–Condon principle to the potentials in fig. 2. The blue tail originates from hard collisions on the repulsive wall of the upper state. Although the Σ–Π free–bound emission is insignificant and is off-scale in the figure, there is an appreciable free–bound component to the Σ–Σ transition, for which the free–bound and free–free intensities at 300 K are comparable for $\Delta \gtrsim 200\ cm^{-1}$. The free–quasibound emission, which we did not calculate, will also contribute to the Σ–Σ blue tail. The total free–quasibound contribution is readily calculated as the difference between the total free emission coefficient (11) from closure and the sum of the integrated free–free and free–bound coefficients in fig. 4. At 300 K the free–free, free–bound, and free–quasibound contributions to the total Σ–Σ K_f are 73, 20, and 7% respectively. Thus the blue tail in fig. 3 will be enhanced by $\approx$10% for $\Delta \gtrsim 200\ cm^{-1}$ if the free–quasibound contribution were added. As temperature is increased, the free–bound and free–quasibound fraction of the total emission will decrease and the free–free fraction will increase.

Table 2
ArO total effective two-body emission coefficient[a]

T(K)	K_f	K_b[b]	K	Measured K
78	2.26	1.78	4.04	
300	2.56	0.17	2.73	3.9[c], 5.1[d], 4.7[e], 4.6[f]
600	2.89	0.06	2.95	

a) In units of $10^{-18}\ cm^3\ s^{-1}$.
b) Does not include quasibound–bound. See text.
c) Cunningham and Clark [6].
d) Corney and Williams [7].
e) Sharpless, Slanger and Black [8].
f) Atkinson and Welge [9].

Table 2 shows our calculated total two-body emission coefficient K at several temperatures and a comparison with several experimental measurements at room temperature. The calculated K is 40% smaller than the average of the three measured values. This represents satisfactory agreement given the approximate model employed.

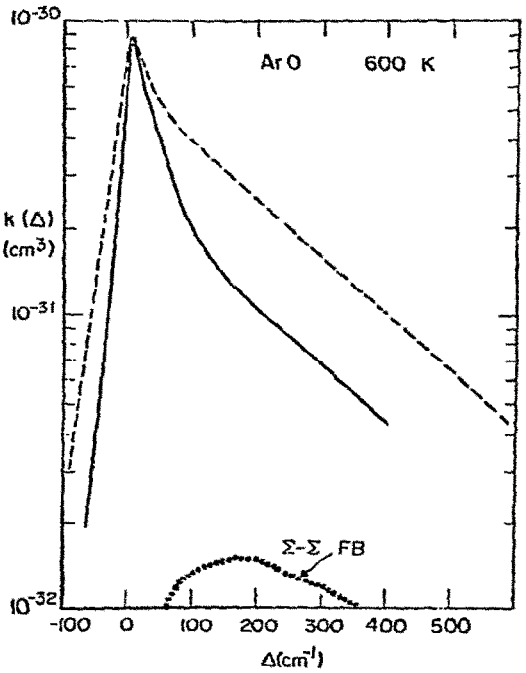

Fig. 5. Calculated ArO emission profile at 600 K (solid line). The dashed line shows the experimental spectrum of Powell and Murray [22] at an estimated temperature of 500–600 K. The calculated Σ–Σ free–bound emission is also shown (dotted line).

The ArO emission continuum has recently been measured at elevated temperatures (≈500–600 K) [22]. Fig. 5 shows our calculated profile $k(\Delta)$ at 600 K and the experimental relative shape profile normalized to a total emission coefficient of $5.0 \times 10^{-18}\,cm^3\,s^{-1}$, found by scaling the average 300 K coefficient $4.6 \times 10^{-18}\,cm^3\,s^{-1}$ by the ratio of our calculated 600 K and 300 K coefficients. The experimental spectrum (dispersion 1.7 Å/mm) did not show any significant line emission features. The calculated and experimental magnitudes at the line center are close, but there are appreciable differences elsewhere. The experimental spectrum is broader near the peak and has a more intense blue tail than calculated. We believe that a major source of error in the calculation is in short range overlap effects on the transition moment to the left of the van der Waals minimum. These tend to increase the $\Sigma-\Sigma$ moment and decrease the $\Sigma-\Pi$ moment. In addition, the dispersion potentials will not be the same for $O\,^1S$ and $O\,^1D$. The result of these two effects will be to put more emphasis on hard collisions relative to long range collisions, and to decrease the $\Sigma-\Pi$ contribution relative to the $\Sigma-\Sigma$. The greater contribution from hard collisions where the $\Sigma-\Sigma$ transition moment is larger than in the model is expected to broaden the peak and greatly enhance the blue tail, as observed. The smaller calculated total emission coefficient relative to measurement implies that the increase in the $\Sigma-\Sigma$ transition moment is more important than the decrease in the $\Sigma-\Pi$ moment.

In spite of its simplicity, the long range T_4/R^4 transition moment permits a simple qualitative understanding of the relative two-body emission coefficients of oxygen ^1S and sulphur ^1S with various rare gas partners R, except Xe for which the emission is almost entirely bound–bound [5,6]. The peak contribution to the sum (12) comes from rotational quantum number J corresponding to impact parameters near the minimum R_m of the upper potential. If we assume the positions of the $O\,^1S-R$ minima are nearly the same for rare gas partners He through Kr, as is true for Ne–R pairs [11], then the ratio $K(A^*-R)/K(A^*-Ar)$ depends only on the rare gas polarizability ratio $[\alpha(R)/\alpha(Ar)]^2$. These ratios are the same whether the metastable A^* is $O\,^1S$ or $S\,^1S$. This ratio is shown in table 3 along with the ratios of various experimentally measured emission coefficient. The qualitative variations are in good agreement. The quantitative comparison is better than would be expected from such a simple-minded approach and must to some extent be fortuitous.

Table 3
Relative total emission coefficients

	$K(A^*-R)/K(A^*-Ar)$				
	$A^* = O\,^1S$			$A^* = S\,^1S$	$\left(\frac{\alpha(R)}{\alpha(Ar)}\right)^2$
R	ref. [8]	ref. [9]	ref. [7]	ref. [8]	
He	0.015	0.023		0.013	0.015
Ne		0.071	0.070		0.058
Ar	1.00	1.00	1.00	1.00	1.00
Kr	5.1	4.1		3.6	2.3

In a similar manner, the ratio $K(S\,^1S-R)/K(O\,^1S-R)$ of sulphur and oxygen ^1S emission coefficients with the same rare gas partner is predicted to be independent of the rare gas partner. The S/O ratio is determined by three effects: (1) the ratio of the square of the quadrupole moments, (2) the ratio of ν^3 factors, and (3) the substantially larger R_m expected in the rare gas sulphides since the larger physical size of the sulphur relative to oxygen leads to a much larger long range repulsion not compensated by the increased dispersion energy. If we assume that R_m increases from 6.5 au in ArO to 7.5 au in ArS corresponding to the 1.0 au increase in $\langle r \rangle$ from oxygen to sulphur, then the reduction in t^2 is 0.32. This leads to a $K(O\,^1S-R)/K(S\,^1S-R)$ ratio of 0.8, which agrees well with measured ratios of 0.8, 0.9, and 0.6 for R = He, Ar, and Kr respectively [8].

4. Summary

In summary, we have presented a theory to explain the main features of the $O\,^1S$ collision-induced green emission in rare gases. Approximate model potentials were constructed for ArO by adding the long-range dispersion energy to the repulsive overlap interaction calculated from the first order wavefunction. The transition moment is the quadrupole-induced dipole term T_4/R^4. The theory accounts for the main features of the bound–bound spectrum, predicts a total ArO two-body emission coefficient only 40% less than measured, and predicts an emission profile at least in qualitative agreement with experiment. The theory enables us to understand qualitatively the relative two-body emission

coefficients of O^1S and S^1S with various rare gas partners. The most significant improvement to this theory would be to include short-range overlap effects on $t(R)$. The theory also indicates that an experimental high resolution study of the bound–bound ArO and KrO spectra at liquid N_2 temperature would be very helpful in improving our understanding of these rare gas oxide excimers.

Acknowledgement

This work was sponsored by ERDA. We wish to thank Drs. H.T. Powell and J.R. Murray of Lawrence Livermore Laboratory for providing their ArO emission spectrum prior to publication. We also thank Drs. F.H. Mies and K.M. Sando for beneficial discussions.

References

[1] H.T. Powell, J.R. Murray and C.K. Rhodes, Appl. Phys. Letters 25 (1974) 730.
[2] H.T. Powell, Lawrence Livermore Laboratory, Laser Program Annual Report, UCRL-50021 (1974).
[3] J.R. Murray and P.W. Hoff, in: High energy lasers and their applications, eds. S. Jacobs, M. Sargent III and M.O. Scully (Addison-Wesley, Reading, 1974).
[4] C.D. Cooper and M. Lichtenstein, Phys. Rev. 109 (1958) 2026.
[5] C.D. Cooper, G.C. Cobb and E.L. Tolnas, J. Mol. Spectry. 7 (1961) 223.
[6] D.L. Cunningham and K.C. Clark, J. Chem. Phys. 61 (1974) 1118.
[7] A. Corney and O.M. Williams, J. Phys. B5 (1972) 686.
[8] G. Black, R.L. Sharpless and T.G. Slanger, J. Chem. Phys. 63 (1975) 4546.
[9] R. Atkinson and K.H. Welge, J. Chem. Phys. 63 (1975), to be published.
[10] F.H. Mies, Mol. Phys. 26 (1973) 1233.
[11] J.S. Cohen and R.T Pack, J. Chem. Phys. 61 (1974) 2372.
[12] H.F. Schaefer III, J. Chem. Phys. 54 (1971) 2207.
[13] G. Das and A.C. Wahl, J. Chem. Phys. 56 (1972) 1769.
[14] H.L. Kramer and D.R. Herschbach, J. Chem. Phys. 53 (1970) 2792.
[15] M.B. Doran, J. Phys. B7 (1974) 558.
[16] W.J. Stevens and F.P. Billingsley II, Phys. Rev. A8 (1973) 2236.
[17] G. Starkschall and R.G. Gordon, J. Chem. Phys. 54 (1971) 663.
[18] J.P. Desclaux, Atomic Data Nuclear Data Tables 12 (1973) 312.
[19] D.M. Whisnant and W. Byers-Brown, Mol. Phys. 26 (1973) 1105.
[20] C. Cuthbertson and M. Cuthbertson, Proc. Roy. Soc. A135 (1967) 40.
[21] R.A. Gordon, J. Chem. Phys. 51 (1969) 14.
[22] H.T. Powell and J.R. Murray, private communication (1975).